TISSUE ENGINEERING: Part A
Volume 22, Numbers 5 and 6, 2016

DOI: 10.1089/ten.tea.2015.0503

termis
Tissue Engineering
& Regenerative Medicine
International Society

ORIGINAL ARTICLE

Elasticity Modulation of Fibroblast-Derived Matrix for Endothelial Cell Vascular Morphogenesis and Mesenchymal Stem Cell Differentiation

Ping Du, PhD,[1,2,*] Muhammad Suhaeri, MS,[1,2,*] Ramesh Subbiah, MS,[1,2] Se Young Van, MS,[1,2] Jimin Park, MS,[1] Sang Heon Kim, PhD,[1,2] Kwideok Park, PhD,[1,2] and Kangwon Lee, PhD[3,4]

Biophysical properties of the microenvironment, including matrix elasticity and topography, are known to affect various cell behaviors; however, the specific role of each factor is unclear. In this study, fibroblast-derived matrix (FDM) was used as cell culture substrate and physically modified to investigate the influence of its biophysical property changes on human umbilical vein endothelial cells (HUVECs) and human mesenchymal stem cells (hMSCs) behavior *in vitro*. These FDMs were physically modified by simply storing them at different temperatures: the one stored at 4°C, maintained its original properties, was considered natural FDM, whereas the ones stored at −20°C or −80°C, exhibited a distinct surface morphology, were considered physically modified FDM. Physical modification induced matrix fiber rearrangement in FDM, forming different microstructures on the surface as characterized by focused ion beam (FIB)-cryoSEM. A significant increase of matrix elasticity was found with physically modified FDMs as determined by atomic force microscopy. HUVEC and hMSC behaviors on these natural and physically modified FDMs were observed and compared with each other and with gelatin-coated coverslips. HUVECs showed a similar adhesion level on these substrates at 3 h, but exhibited different proliferation rates and morphologies at 24 h; HUVECs on natural FDM proliferated relatively slower and assembled to capillary-like structures (CLSs). It is observed that HUVECs assembled to CLSs on natural FDMs are independent on the exogenous growth factors and yet dependent on nonmuscle myosin II activity. This result indicates the important role of matrix mechanical properties in regulating HUVECs vascular morphogenesis. As for hMSCs multilineage differentiation, adipogenesis is improved on natural FDM that with lower matrix elasticity, while osteogenesis is accelerated on physically modified FDMs that with higher matrix elasticity, these results further confirm the crucial role of matrix elasticity on cell fate determination.

Introduction

Cell or tissue-derived extracellular matrix (ECM)-based biomaterials, provided with inherently complex biochemical and biophysical properties, have been widely used in tissue engineering. Studies have demonstrated that cell-derived matrices (CDMs) from human lung fibroblast[1] and from a coculture of dermal fibroblast with breast cancer cell line[2] supported human umbilical vein endothelial cells (HUVECs) vascular morphogenesis *in vitro*. We previously reported that mouse fibroblast-derived matrix (FDM) and preosteoblast-derived matrix provided an excellent platform for HUVECs and rat bone marrow stromal cell adhesion, proliferation, and differentiation *in vitro*.[3,4] Those studies provide as good examples in demonstrating the importance of presenting the cells with appropriate niche, which CDMs naturally possess.

Considering the significance of mechanical property and appropriate cellular niche, we developed a system that incorporates the impact of mechanics using native ECM. FDM was used to provide the cell with natural microenvironment, whereas mechanical cue was incorporated by temperature treatment to FDM. We found that by keeping FDM in freezing temperatures (−20°C and −80°C), it changes its

[1]Center for Biomaterials, Korea Institute of Science and Technology, Seoul, Republic of Korea.
[2]Department of Biomedical Engineering, Korea University of Science and Technology, Daejeon, Republic of Korea.
[3]Program in Nanoscience and Technology, Graduate School of Convergence Science and Technology, Seoul National University, Seoul, Republic of Korea.
[4]Advanced Institutes of Convergence Technology, Gyeonggi-do, Republic of Korea.
*These two authors contributed equally to this work.

mechanical property; lower temperature treatment gave rise to higher matrix elasticity. Hence, we investigated the effect of mechanical cues on cell behaviors by using a more appropriate cell culture substrate. This method of physical-based modification is simpler and milder than the chemical based, such as cross-linking using genipin,[5] glutaraldehyde,[6] 1-Ethyl-3-(3-dimethylaminopropyl) carbodiimide hydrochloride,[7] and transglutaminase.[8]

We hypothesize that the mechanical changes to FDM induced by temperature treatment would affect cellular responses. To test our hypothesis, we cultured HUVECs and human mesenchymal stem cells (hMSCs) on natural FDM and modified FDM (stored in −20°C and −80°C) with gelatin or tissue culture plate (TCP) as control. The biophysical and biomechanical properties of FDMs were thoroughly investigated using focused ion beam (FIB)-cryoSEM and atomic force microscopy (AFM). The cellular responses of HUVECs and hMSCs, including cell adhesion, proliferation, morphology, and differentiation, were investigated. This study is the first reported physical modification on CDM, and the different cellular responses of HUVECs and hMSCs suggested that the current system could be a useful and convenient research material for various applications.

Materials and Methods

Preparation of FDM and its physical modification

NIH3T3 mouse fibroblasts (ATCC) were cultured in Dulbecco's modified Eagle's medium (DMEM) supplemented with 10% fetal bovine serum (FBS), 100 U/mL penicillin, and 100 μg/mL streptomycin (Invitrogen). Fibroblasts were seeded at a density of $2\times10^4/cm^2$ on gelatin-coated glass coverslips in 12-well plates, and cultivated for 5 or 6 days until confluence. For gelatin coating, gelatin type B (G-9391; Sigma-Aldrich) was dissolved in distilled water (0.5%, w/v) and then sterilized in an autoclave at 120°C for 15 min. Sterilized glass coverslips (18-mm diameter) were placed into 12-well plates and incubated with the gelatin solution (0.5 mL/well) at least for 15 min in incubator, after which the gelatin solution was aspirated and gelatin-coated coverslips were air dried before cell seeding. The medium was changed every 2 or 3 days. For decellularization, the confluent cells were treated briefly with a detergent solution containing 0.25% Triton X-100 and 50 mM NH_4OH (Sigma-Aldrich). After the samples were washed with phosphate-buffered saline (PBS), the mixture of 50 U/mL DNase I and 2.5 μL/mL RNase A (Invitrogen) in PBS was added, incubated at 37°C for 1–2 h, and the decellularized samples were then gently washed twice with PBS.

For physical modification, FDM samples in PBS were stored in refrigerator at different temperatures, that is, 4°C, −20°C, and −80°C overnight, and then thawed at room temperature. FDMs stored at 4°C maintained their original properties and were considered natural ones. The resulting samples were named as FDM, FDM (−20), and FDM (−80), respectively. Surface morphology of these FDMs was observed under a phase-contrast microscope (Zeiss Axio Vert.A1).

Characterization of FDMs using FIB-cryoSEM and AFM

The surface structure and topography of FDMs before and after physical modification were observed by the cryo-SEM/FIB equipment (Quanta 3D FEG; FEI) with an Alto 2500 cryo-transfer system (Gatan). FDM samples were loaded on a copper stub and subsequently submerged into liquid nitrogen slush. After 30 s, the samples were transferred to the preparation chamber at a pressure of 10^{-5} mbar under −190°C. The metal deposition was then performed with a current of 5 mA for 100 s in the same chamber. The coated samples were transferred into the microscope chamber at a pressure of 10^{-5} mbar under −190°C. Samples were photographed in normal mode at 5 kV accelerating voltage and 11.8 pA current. Regions of interest were cryosectioned by Ga ion beam at 30 kV accelerating voltage and 3 nA current. Surface morphology after FIB section was imaged using the same parameters as mentioned above. The morphology of porosity in FDM surface was quantitatively analyzed using image J software by two parameters: pore diameter and aspect ratio, the quantification data were obtained from five different regions in each sample ($n=3$, each group).

For biophysical characterization, FDMs were tested in a liquid contact mode using Nanowizard II bio-AFM (JPK Instruments). The combined inverted optical stage helps to precisely position the AFM tip over the region of interest on FDM. A hydra2R-50NG AFM probes (AppNano) was used to scan FDM morphology. The data obtained from the Bio-AFM height scale images were used to calculate the surface roughness of FDMs. For biomechanical characterization, a sphere tip (5 μm diameter) on silicon nitride (Si_3N_4) cantilever with the spring constant of 0.01 N/m (PT.SiO_2.AU.SN.5; Novascan Technologies, Inc.) was used. Young's modulus (YM) was measured by the nanoindentation method. The indentation forces (0.5–10 nN) were applied during the tests to find out a proper indentation depth ranging from 50 to 500 nm. Both tip–sample separation curves and YMs (10 different regions in each sample, $n=3$) were subsequently obtained according to Hertz's contact model using JPK data processing software (v3.3.25). The poison ratio of the FDMs was considered to be 0.5 (JPK Instruments). Following the JPK manual instruction, the average YM of each FDM was calculated from the average loads when the indentation depth reaches 10–20% of the matrix thickness.

HUVECs culture and proliferation assay

HUVECs (C2517A; Lonza) were cultured in an endothelial cell growth medium (EGM-2 BulletKit, CC-3162) at 37°C under a 5% CO_2 humidified atmosphere. The HUVECs between passage 4 and 6 were used in this study. To investigate cell proliferation level, HUVECs (5×10^4/well) suspended in the EGM-2 medium were seeded on the gelatin-coated coverslips (control), FDM, FDM (−20), and FDM (−80) in 12-well plates ($n=3$, each group), respectively. FDMs were rinsed with PBS thrice before cell seeding. Cell attachment level at 3 h and cell proliferation level at 24 and 72 h were analyzed by the Cell Counting Kit-8 (CCK-8, CK04; Dojindo) assay. Briefly, 10% CCK-8 solution in culture medium was added to each sample and incubated at 37°C for 2 h. Aliquots of each sample (100 μL) were transferred to a 96-well plate and the absorbance was measured at a wavelength of 450 nm using a multiskan microplate reader (Thermo Fisher Scientific). Cell proliferation assays were performed in triplicate. In addition, after cultivation of HUVECs on each substrate for 24 h, samples

were fixed and dehydrated for SEM scanning to observe cell attachment and cell morphology on the FDM.

HUVECs adhesion and morphology analysis

To further analyze HUVECs adhesion and morphology on different substrates, cells were seeded at a density of 1×10^4 cells/cm^2 on gelatin-coated coverslips, FDM, FDM (−20), and FDM (−80). After cultivation for 24 h in the EGM-2 medium, HUVECs were fixed by cold acetone and subjected to immunofluorescence staining (IFS) against vinculin and F-actin. In brief, samples were washed by PBS thrice and blocked with 3% bovine serum albumin (BSA) in PBS, followed by overnight incubation with primary antibody against mouse monoclonal vinculin (sc-73614; Santa Cruz Biotechnology) diluted in 1% BSA (1: 300). After washing, those samples were treated with secondary antibody of Alexa Fluor® 488 F(ab') fragment of goat anti-mouse IgG (A-11017) and TRITC (Tetramethylrhodamine isothiocyanate)-conjugated phalloidin (A415; Life Technologies) (1: 200) for 1 h at room temperature. Immunostained samples were washed thrice and then mounted on microscope slides using the vectashied® mounting medium with DAPI (H-1200; Vector Laboratories, Inc.) for nucleic labeling. Images were taken under a fluorescence microscope (Zeiss Axio Vert.A1) at 400 magnification. Cell morphology was quantitatively assessed by cell spreading area and aspect ratio. Quantification data were obtained by manually outlining cell borders (10–15 cells) per sample ($n = 3$) and processed by image J software.

Cell migration—wound healing assay

To investigate cell motility, HUVECs were seeded at a high density of 1×10^5 cells/well on three types of FDMs in 12-well plates and cultivated in the EGM-2 medium (CC-3162) for 2 days until confluence. The confluent layers of HUVECs were carefully scratched using a pipette tip (1 mL) to create an artificial wound. The samples were then washed twice with PBS to remove the cell debris and cultivated in the endothelial basal medium-2 (EBM-2, CC-3156) with the supplement of 2% FBS and 50 ng/mL recombinant human stromal cell-derived factor-1 alpha (SDF-1α; chm-262; Prospec). Samples were placed under Cell Observer® with live-cell imaging microscopy (Zeiss Axio Vert.A1) for 24 h with a scanning interval of 10 min to monitor cell migration and repopulation in the scratched area. The repopulation speed of cells on each substrate was evaluated by the average wound closure percentage after 6 and 12 h, respectively. Quantitative data were obtained from six areas per sample ($n = 3$). Experiments were performed in triplicate.

Quantitative polymerase chain reaction

For quantitative polymerase chain reaction (qPCR) analysis, HUVECs were cultured for 24 h on different substrates with the stimulation of 50 ng/mL SDF-1 in the EBM-2 medium with 2% FBS. Total mRNA was extracted from the HUVECs using Trizol® RNA isolation reagents (Invitrogen), following the manufacturer's instruction. Concentration and purity of the isolated mRNA were determined using a NanoDrop ND-1000 spectrophotometer (Thermo Fisher Scientific). One microgram mRNA and diethylpyrocarbonate (DEPC)-treated water was added to the Maxime RT PreMix Kit (25081; Intron) tubes to a total volume of 20 μL. Samples were then subjected to cDNA synthesis at 45°C for 60 min and RTase inactivation at 95°C for 5 min. The resulting cDNA product (1 μL), 10 pmol of each reverse and forward primer in 2 μL sterile DW, 10 μL of SYBR Green real-time PCR mix (RR420A; Takara), 0.4 μL of ROX reference dye, and 6.6 μL DW were mixed in PCR reaction tubes (Applied Biosystems) to a total volume of 20 μL. The reaction reagents were mixed thoroughly, centrifuged briefly, and then placed in a real-time cycler (7500 Real-Time PCR System; Life Technologies™); reaction proceeded at a condition of initial denaturation and DNA polymerase activation at 95°C for 5 min, followed by 40 cycles of denaturation at 95°C for 10 s, and annealing/extension at 58°C for 34 s. Target genes and their primer sequences were membrane type 1-matrix metalloproteinase (*MT1-MMP*): GCAGAAGTTTTACGGCTTGC (forward) and TCT CAGCCCCAAACTTGTCT (reverse); and chemokine (C-X-C motif) receptor 4 (*CXCR4*): CTCCAAGCTGTCACACTCCA (forward) and GTCGATGCTGATCCCAATGT (reverse). Glyceraldehyde-3-phosphate dehydrogenase (*GAPDH*) was used as housekeeping gene and the primer sequence is GGCTCTCCAGAACATCATCC (forward) and TTTCTA-GACGGCAGGTCAGG (reverse).

Nonmuscle myosin II activity and HUVEC morphology

HUVECs (5×10^4 cells/well) in EGM-2 were seeded on three types of FDMs, along with gelatin-coated coverslips as control group in 12-well plates ($n = 8$). For nonmuscle myosin II (NMM II) activity inhibition, Blebbistatin (B0560; Sigma-Aldrich) dissolved in DMSO was added to the HUVEC culture medium to a final concentration of 50 μM. Correspondingly, HUVECs treated by same volume of DMSO without Blebbistatin ($n = 4$, each group) were used for comparison. The treatment with or without Blebbistatin was started after 24-h cultivation and lasted for 30 min. Cells were fixed, washed, and permeabilized for CD31 (PECAM-1) and F-actin staining. In brief, samples were first blocked with 3% BSA in PBS and then incubated with primary antibody of rabbit polyclonal anti-CD31 (ab28364; Abcam) overnight. After washing thrice, secondary antibody of goat polyclonal anti-rabbit IgG-H&L Dylight 488 (ab96899) and TRITC-conjugated phalloidin (A415) was applied to visualize CD31 and cytoskeleton. The stained samples were mounted on microscope slides in a mounting medium with DAPI (H-1200) and examined under confocal laser scanning microscopy (LSM 700; Carl Zeiss). To identify a lumen structure formation, consecutive z-stack images (10–25 iterations) with an interval thickness of 1 μm at 400 magnification were acquired and a three-dimensional (3D) reconstruction of capillary-like structure (CLS) was performed using Imaris software (Imaris 7.1). Cross-sectional views of reconstructed images showed a hollow structure of lumen.

HUVEC morphology without exogenous growth factors

To investigate whether HUVEs morphology on FDMs and gelatin-coated coverslips is dependent on chemical supplements in culture medium, HUVECs (5×10^4 cells/well) were cultured in the EBM-2 medium (CC-3156) without adding any supplements and growth factors (EGM-2 SingleQuot Kit Suppl. & Growth Factors, CC-4176; Lonza). The EGM-2 SingleQuot Kit comprised hEGF, 0.5 mL; VEGF, 0.5 mL; R3-IGF-1, 0.5 mL; Ascorbic Acid, 0.5 mL; Hydrocortisone,

0.2 mL; hFGF-β, 2.0 mL; Heparin 0.5 mL; FBS, 10.0 mL; and GA, 0.5 mL. Cell morphology was imaged at 24 h under a phase-contrast microscope. To further compare HUVEC morphology on natural FDM with or without supplements and growth factors, HUVECs on natural FDM at 24 h ($n = 3$, each group) were fixed, washed, and permeabilized for F-actin staining. In brief, cells were first incubated with TRITC-conjugated phalloidin (A415) in 1% BSA for 20 min. After washing thrice, samples were then mounted on microscope slides in a mounting medium with DAPI (H-1200) for imaging under a fluorescence microscope (Zeiss Axio Vert.A1).

hMSC morphology and proliferation assay

hMSCs (Lonza) passage 7–9 were seeded at a density of 2.1×10^4 cells/cm^2 and cultured under a basal medium (PT-3238; Lonza) at 37°C and 5% CO_2. After 1 day, samples were harvested and fixed with 4% formaldehyde. Cells were permeabilized with 0.1% Triton-X 100 and blocked with 1% BSA for 1 h. Cell cytoskeleton was stained with Rhodamine phalloidin (R415) for 20 min, mounted, and observed under fluorescence microscope (CKX-41; Olympus). As much as 20 cells for each group were analyzed for cell spreading area and cell circularity index (values range 0–1 with value 1 indicating perfect circle). Cell proliferation was carried out at day 1 and 3 using the Cell Counting Kit-8 (CK04; Dojindo) following same protocol described in Cell Migration—Wound Healing Assay section.

hMSC adipogenesis and osteogenesis

For differentiation, cells were cultured to confluence and the medium was changed into a differentiation medium, which consists 0.5 μM dexamethasone (D4902; Sigma-Aldrich), 0.5 μM isobutyl methylxanthine (I7018; Sigma-Aldrich), and 50 μM indomethacin (I7378; Sigma-Aldrich) for adipogenic induction, whereas for the osteogenic medium, the supplements were 10 nM dexamethasone, 20 mM β-glycerophosphate (G9422; Sigma-Aldrich), 25 μg/mL ascorbic acid (A4403; Sigma-Aldrich), and 50 ng/mL BMP-2 (R&D system). Differentiation was carried out for 2 weeks with medium change every 2–3 days. Upon completion of differentiation, cells were washed with PBS and fixed with 10% formaldehyde for 1 h. After that, they were stained for 20 min with 5 μg/mL oil red O (198196; Sigma-Aldrich) and 0.01 g/mL alizarin red S (A5533; Sigma-Aldrich) for detection of lipid droplet and calcium, respectively. After washing, the samples were observed under microscope (Carl Zeiss) and 15 random images from three replicates in each group were quantified.

Statistical analyses

Statistical analyses of the data were performed using one-way analysis of variance (ANOVA), with Tukey's *post hoc* multiple comparisons (GraphPad Prism 5). All the data represented the mean values and standard deviations. Statistical significance was determined as $*p < 0.05$, $**p < 0.01$, and $***p < 0.001$, respectively.

Results and Discussion

Biophysical property changes on FDM induced by physical modification

The topographic features of substrates in microscale or nanoscale have a great influence on cell behaviors, thus characterizations of these features are of critical importance.[9] FDM samples were thoroughly characterized by different methods in microscales and nanoscales. Under phase-contrast microscope, natural FDM exhibited homogeneously distributed fibers that were thin and dense. In contrast to the natural ones, FDM (−20) comprised interconnected fiber networks forming mesh-like structures with various sizes of fibers on the surface. Similar pattern of microstructures was detected on the surface of FDM (−80), but they were denser and smaller (Fig. 1A, inset). It is likely that matrix fiber rearrangement on physically modified FDM is caused by ice crystal formation during freezing at low temperature.[10] This kind of surface morphology changes of FDM could also be caused by the contraction of the ECM proteins and their dehydration at freezing temperature.[11]

For a more detailed analysis, we employ FIB-cryoSEM to visualize the inner microstructures of FDMs. Porous structures were observed on the surface of all the FDMs in the frozen hydrated state by FIB-cryoSEM. Natural FDMs exhibited larger porosities aligned in longitudinal direction compared with those on physically modified ones, whereas FDM (−80) and FDM (−20) exhibited circular and interconnected porous structures. Interestingly, much smaller pores were rich in FDM (−80) than in FDM (−20) (Fig. 1A). To observe the inner structure of FDMs, the surfaces were milled by FIB and scanned again at a higher resolution. Similar porous structures were observed throughout the whole thickness of FDMs (Fig. 1B). Scanned under much higher resolution, uniform and tiny porous structures were observed on FDM (−80) (Fig. 1A, B). When the diameters of porous structure were quantitatively analyzed using Image J software, the values were 3.02 ± 0.85, 1.03 ± 0.15, and 0.52 ± 0.15 μm for FDM, FDM (−20), and FDM (−80), respectively (Fig. 1C). The pore diameters are significantly different among three types of FDMs, and that in FDM (−80) is the smallest. This result agrees with the previous finding that different freezing temperatures give rise to different pore diameters to alginate scaffold and pore diameters are reduced with decreasing freezing temperatures.[12] To further describe the different surface morphology of FDMs, the aspect ratio of pore is quantitatively analyzed using image J software, the value of that is 3.8 ± 0.96, 1.45 ± 0.36, and 1.39 ± 0.23 with FDM, FDM (−20), and FDM (−80), respectively (Fig. 1D). Therefore, it can be concluded that the pores on natural FDM are more elongated than those on physically modified FDM.

AFM can present the detailed surface information of FDMs, including roughness, topography with a scanning area of 100×100 μm. Natural FDM showed aligned longilineal porous structures, whereas physically modified FDMs exhibited small circular porosity (Fig. 2A). The surface morphology observed by AFM is consistent with that observed by FIB-cryoSEM. Furthermore, it was found that the average roughness of FDM, FDM (−20), and FDM (−80) were 89.8 ± 25.8, 95.1 ± 8.7, and 266.6 ± 13.4 μm, respectively. A significant higher roughness was found with FDM (−80) than that with both FDM (−20) and FDM (Fig. 2B). The AFM nanoindentation analysis further presented that physical modification significantly increased the elasticity of FDM; the average YM of FDM, FDM (−20), and FDM (−80) was 83.3 ± 17.2, 564.8 ± 143.5, and 4313.3 ± 1353.1 Pa, respectively (Fig. 2C). FDM (−80) with the smallest pore size has

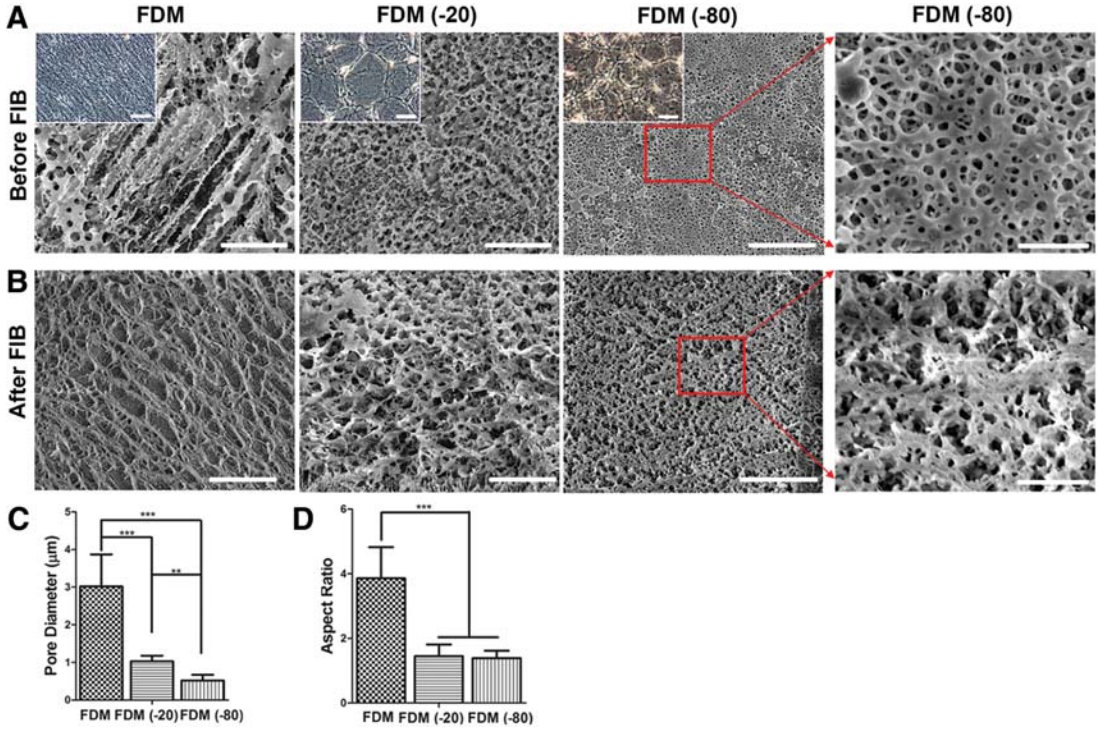

FIG. 1. FDM characterization by FIB-cryoSEM. Surface morphology of FDM, FDM (−20), and FDM (−80) was observed under cryoSEM **(A)** and phase-contrast microscope **(A**, *inset***)**. Samples were scanned under cryoSEM after FIB section **(B)**. Scale bars for **(A)** and **(B)** are 20, 50 (*inset* **A)** and 4 μm (enlarged rectangular of FDM [−80]). Quantitative analysis of pore diameters **(C)** and aspect ratios **(D)** is based on cryoSEM images after FIB cutting. Statistically significant differences among FDMs are indicated as $^{**}p<0.01$ and $^{***}p<0.001$. FDM, fibroblast-derived matrix; FIB, focused ion beam. Color images available online at www.liebertpub.com/tea

the highest matrix elasticity (Figs. 1 and 2C), this observation is consistent with the previous report that matrix stiffness is inversely correlated with pore size.[13] In summary, it is found that physical modification on FDM induced matrix fiber rearrangement, which consequently alters surface structures and increased matrix elasticity of FDMs.

HUVEC behavior on physically modified FDMs

To evaluate the impact of FDM physical modification on HUVEC behavior, cells were seeded on three types of FDMs and gelatin-coated coverslips. HUVECs attached and spread on all substrates as indicated by SEM images of cells

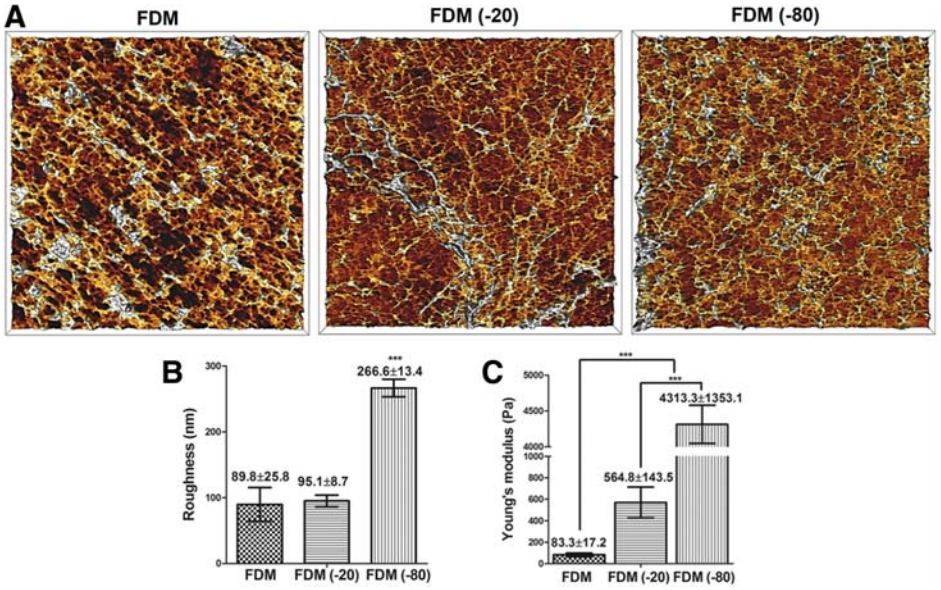

FIG. 2. Biophysical characterization of FDMs. Atomic force microscopy demonstrated porous structure of FDM surface in a scan area of $100\times100\,\mu m^2$ **(A)**. Quantitative data of FDM surface roughness obtained from 12 areas ($n=5$) **(B)**. The average YM of each FDM is calculated from the average loads when the indentation depth reaches 10–20% of the matrix thickness **(C)**. Statistically significant difference among FDMs is indicated as $^{***}p<0.001$. YM, Young's modulus. Color images available online at www.liebertpub.com/tea

in 24-h postseeding and a close cell–matrix interaction can be observed on all the FDM substrates. It is interesting that cells on gelatin, FDM (−20), and FDM (−80) were observed as groups of 2–15 cells forming localized islands (Fig. 3A, top). This kind of multicellular cluster formation has also been detected on fibronectin-coated coverslips in the previous study.[14] HUVEC morphology on natural FDM is distinct from that on physically modified FDM; they connected to each other forming a CLS. On the other hand, cells on the other substrates are simply gathered. This phenomenon is likely correlated with matrix elasticity indicated by YM (Fig. 2C) as previous study claimed that HUVECs formed CLSs on a compliant substrate with an elasticity less than 1000 Pa.[15] Another interesting finding is that HUVECs on natural FDM have long filopodia protruded each other indicating an active motility (Fig. 3A).

To further investigate HUVEC adhesion on each substrate, we carried out immunostaining of cell adhesion-related proteins. Within 24 h, HUVECs were well attached and spread on all the substrates, with well-developed actin stress fibers and focal adhesion points as indicated by F-actin (red) and vinculin (green) staining, respectively (Fig. 3B). Interestingly, HUVECs exhibited much more elongated morphology on natural FDM over the other groups at 24 h. It was notable that vinculin positive signal of HUVECs on natural FDM was significantly less in 24 h, indicating much weaker cell–matrix interactions compared to that on the other substrates. Moreover, less cytoskeleton filaments were detected with HUVECs on natural FDM compared with that on other substrates (Fig. 3B). The finding that HUVECs developed more focal adhesion points and cytoskeleton fibers on substrates with higher matrix elasticity is well consistent with the previous report.[16] Furthermore, this result is also supported by the previous study that HUVECs respond to differences in substrate stiffness by changing their focal adhesion-related proteins as well as actin stress fibers.[17]

To better compare cell morphology on each substrate, cell spreading area and aspect ratio are quantitatively analyzed using image J software. Cell spreading area on gelatin-coated substrates was the largest and that on natural FDM was the smallest in 24 h (Fig. 3C). Moreover, it is found that cell spreading area increased with the rise of matrix elasticity (Figs. 2C and 3C), which strongly implied a correlation between substrates' mechanical property and HUVEC morphology.[15] The cell aspect ratio is defined as the ratio between long axis and short axis of individual cells, HUVECs on natural FDM had significantly larger aspect ratio than those on the other substrates at 24 h (Fig. 3D). A unique sign of vascular

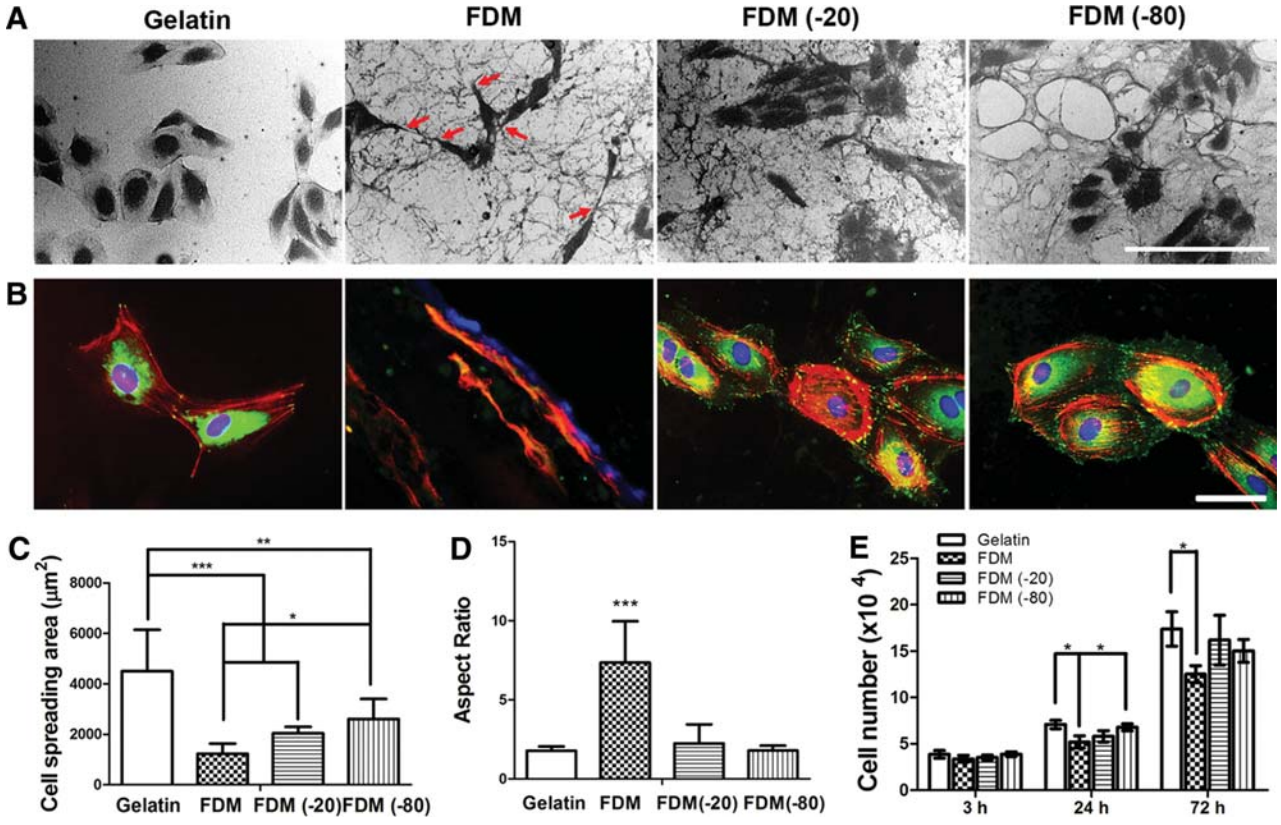

FIG. 3. HUVECs adhesion and morphology analysis. SEM images (500×) of HUVECs adhered on FDM fibers and gelatin-coated coverslips at 24 h. *Arrow* denotes HUVEC filopodia formation on natural FDM **(A)**. Scale bar is 260 μm. HUVEC adhesion and morphology at 24 h was visualized by immunostaining against vinculin (*green*), F-actin (*red*), and DAPI (*blue*) **(B)**. Scale bar is 50 μm. Cell morphology is quantitatively analyzed by cell spreading area **(C)** and cell aspect ratio (the ratio of cell length to width) **(D)**. Cell proliferation on each substrate was analyzed by the CCK-8 assay at 3, 24, and 72 h **(E)**. Statistically significant difference between different substrates is indicated as $*p<0.05$, $**p<0.01$, and $***p<0.001$, respectively. HUVEC, human umbilical vein endothelial cell. Color images available online at www.liebertpub.com/tea

morphogenesis, CLS formation, did not occur on FDM (−20) and (−80), as well as on gelatin, where the average cell aspect ratio on these substrates was less than 3. It has been reported that ECs from large or small diameter blood vessels had different responses to the substrate topography.[18] In this study, we also found that substrate topography affects HUVEC morphology, in which the aspect ratio of HUVECs is directly correlated with FDM porous structure (Figs. 1D and 3D) indicating the additional role of substrate topography on HUVEC morphology. However, different topography cues in substrates without proper stiffness can alter EC adhesion, morphology, migration, and gene expression, but cannot induce CLS formation.[19–22] Our findings imply that CLS formation is strongly linked with matrix stiffness.

About 80% cells were successfully attached on each substrate in 3-h postseeding, suggesting that physical modification of FDM did not affect HUVEC adhesion level. In addition, when cell proliferation level was examined for up to 72 h, it was notable that the proliferation rate of HUVECs on natural FDM was relatively slower than that on the other substrates (Fig. 3E). These results suggested that HUVECs on natural FDMs act as tip cells that tend to form CLSs, whereas HUVECs on physically modified FDMs behave as stalk cells that are proliferative.[23] Furthermore, the result also implied that a balance between HUVEC proliferation and vascular morphogenesis existed.[21]

It is well known that EC migration plays a critical role in the process of angiogenic sprouting and repair of injured vessels.[24,25] Thus, the motility of HUVECs cultured on FDM substrates was examined by wound healing assay, in which the migration process was recorded under a time-lapse microscope. Percentage of wound closure was calculated at 6 and 12 h (Fig. 4A). Compared to the initial wound area at 0 h (Fig. 4A, top), it is visible that after 6 h the wound coverage area was significantly higher on natural FDM than those on physically modified FDM substrates (Fig. 4A, middle). Similar trend of wound coverage level was found after incubation for 12 h (Fig. 4A, bottom). Furthermore, the average wound closure percentage was quantitatively analyzed based on the observations recorded by the time-lapse microscope (Supplementary Videos S1–S3; Supplementary Data are available online at www.liebertpub.com/tea); about 30% wound area was repopulated on natural FDM after 6 h, whereas 10–20% wound area was repopulated on physically modified FDM substrates (Fig. 4B). A similar trend of wound closure was observed after incubation for 12 h and natural FDM showed much faster wound closure than that on physically modified ones. All of this indicated that HUVECs on natural FDM have higher motility than that on physically modified ones and it is supported by the observation that HUVECs formed more filopodia on natural FDM (Fig. 3A). The lower motility of HUVECs on physically modified FDM than other substrates might relate with the matrix elasticity (Fig. 2C), and the strong cell–matrix interaction (Fig. 3B) on physically modified FDM can hinder cell movement. In this study, HUVECs were stimulated by 50 ng/mL SDF-1α with 2% FBS without other supplement and cytokines. Thus, in such a low serum condition and without the supply of mitogen, it can be concluded that cells in the scratched area at 6 and 12 h were caused by HUVEC migration instead of proliferation.

SDF-1α regulates cell migration by binding with chemokine (C-X-C motif)-4 (*CXCR-4*).[26] Additional information for cell migration was sought by investigating gene expression level of *CXCR-4* and matrix remodeling proteolytic enzyme *MT1-MMP* with the stimulation of SDF-1α. *SDF-1α*, secreted from damaged tissues under vascular injuries, is one of the central chemokines involved in vascular repair by regulating vascular cells homing.[27] The results showed that *CXCR-4* was significantly upregulated with

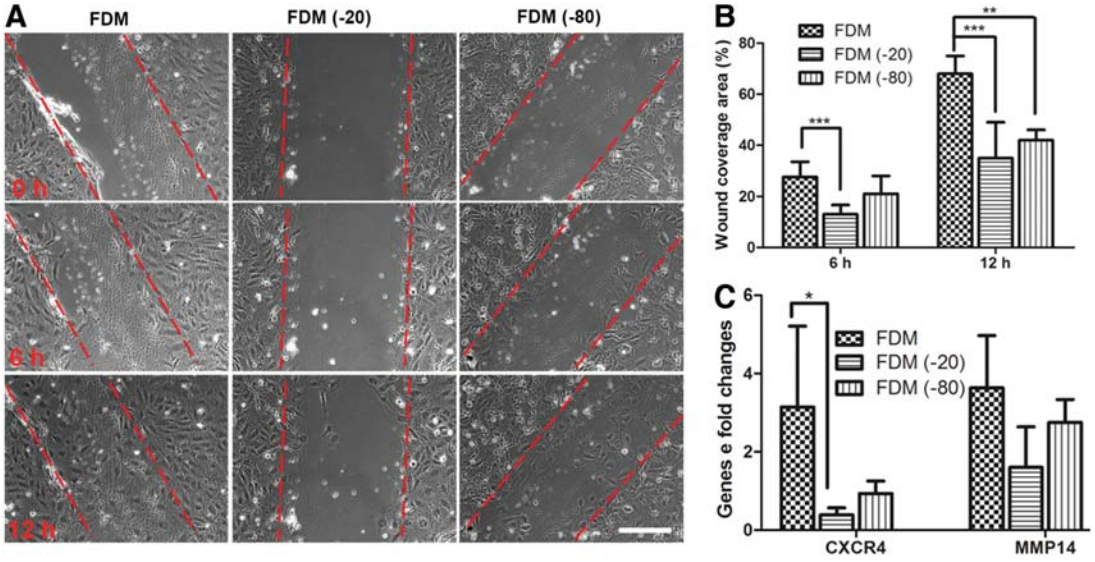

FIG. 4. Cell migration—wound healing assay. Images showed cell migration situation at different time points under time-lapse microscope: *top*, time 0; *middle*, after 6 h; and *bottom*, after 12 h **(A)**. Scale bar is 200 μm. Wound closure percentage after 6 and 12 h was quantitatively analyzed and compared **(B)**. CXCR-4 and MMP-14 gene expression fold changes of HUVECs cultured on different substrates for 24 h **(C)**. Statistically significant difference between gelatin-coated coverslips and FDMs is indicated as $*p < 0.05$, $**p < 0.01$ and $***p < 0.001$, respectively. Color images available online at www.liebertpub.com/tea

HUVECs cultured on natural FDMs and it was statistically significant to that on FDM (−20) (Fig. 4C). *MT1-MMP* has been reported to facilitate neovascularization by degrading the ECM at migrating cell front, thus creating a physical space for cell migration.[28,29] Early study also reported there was much higher expression of *MT1-MMP* on FDM during vascular morphogenesis.[3] Therefore, to examine a correlation between *MT1-MMP* expression and cell migration, the gene expression level of *MT1-MMP* was examined. The trend of *MT1-MMP* on each substrate was consistent with that of *CXCR-4* (Fig. 4C), which implied that both factors might play a crucial role in the movement of HUVECs on FDM.

HUVEC CLS assembly is dependent on NMM II activity

Previous studies demonstrated that cells could sense the surrounding matrix mechanical properties through a NMM II-dependent pathway.[30,31] Consequently, HUVEC morphology on each substrate was observed with or without the inhibition of NMM II activity by adding Blebbistatin in the culture medium. To observe the lumen structure formation of HUVECs, the merged images of CD31, F-actin, and DAPI were reconstructed into 3D configurations by adding the Z-stacks to 2D configuration using Imaris software. The cross-sectional images illustrated 3D lumen hollow structure formed by HUVECs on natural FDM without the treatment of Blebbistatin (Fig. 5A). HUVECs treated by Blebbistatin formed much less density of actin stress fibers compared with that formed by HUVECs without treatment. Moreover, Blebbistatin treatment disrupted the lumen structure that otherwise formed on natural FDM (Fig. 5B). These results demonstrated that CLS formation of HUVECs is dependent on NMM II, the cellular mechanotransducer that could sense the matrix elasticity in the surrounding environment.

Beside biophysical cues, chemical signals such as growth factors and macromolecule compositions have been shown critical in inducing angiogenesis. To eliminate the possibility that the different responses of HUVECs on four substrates is caused by the different growth factor binding capability of each substrate, HUVEC responses on these substrates were further observed by culturing them without adding exogenous growth factors or angiogenic agents. It is found that on all the substrates, the morphology of HUVECs cultured in the medium without supplements was similar with those cultured in the medium together with supplements (Fig. 6A); CLSs were formed on natural FDMs even without supplements (Fig. 6B). This finding indicates that CLSs and filopodia formation on natural FDM is independent on exogenous growth factors or cytokines. In addition to this, the macromolecule compositions of FDM such as fibronectin, laminins, and collagen type I of fresh FDM and physically modified FDM (−80) were compared (Supplementary Fig. S1), it was found that all of these molecules exist even after physical modification. All of the above results showed that the behavior of HUVECs is dominantly affected by matrix elasticity, but not the chemical signals added in culture media or topography of underlying substrate.

Human MSC multilineage specification is dependent on substrate elasticity

To further demonstrate the importance of biophysical cues on cell behavior, MSCs were also used to evaluate the effect of matrix elasticity in FDM on multilineage differentiation of stem cells. The behavior of these cells was assessed based on their morphology, proliferation, and multilineage differentiation into adipogenesis and osteogenesis. Our data show that MSCs behaved differently according to which substrates they

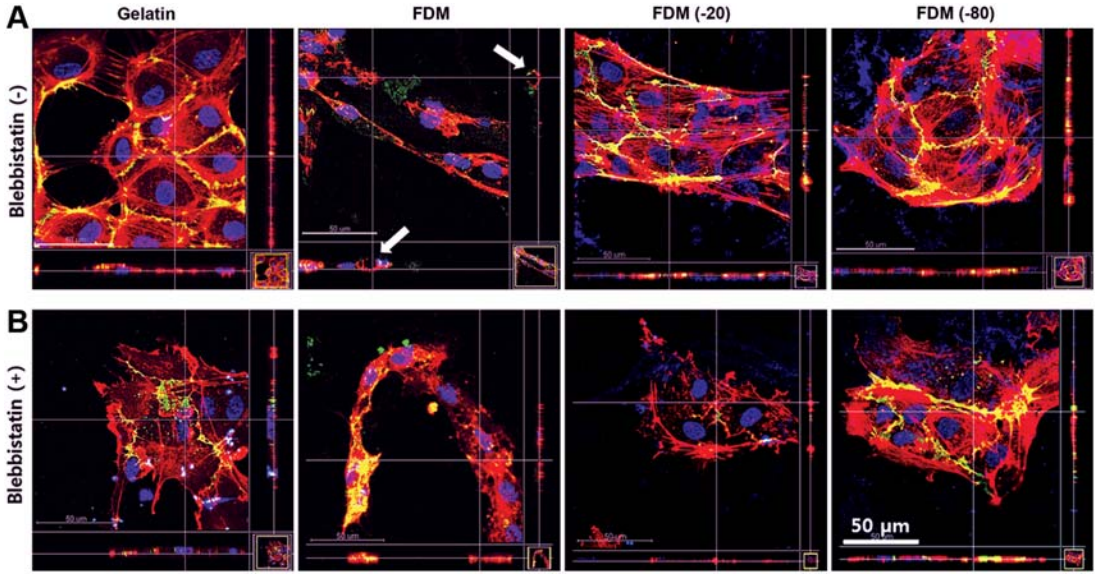

FIG. 5. HUVEC morphology with the inhibition of nonmuscle myosin II activity. HUVECs morphology at 24 h was observed using IFS against CD31 (*green*), along with F-actin (*red*) and DAPI (*blue*). CLSs were observed on natural FDM, and capillary lumen indicated by *white arrow* was only detected on natural FDM based on three-dimensional reconstructed confocal microscope images **(A)**. With 50 μM Blebbistatin treatment for 30 min at 24 h, cytoskeleton fibers were significantly reduced on all the substrates and capillary lumen on natural FDM was disrupt **(B)**. Scale bar is 50 μm. CLS, capillary-like structure; IFS, immunofluorescence staining. Color images available online at www.liebertpub.com/tea

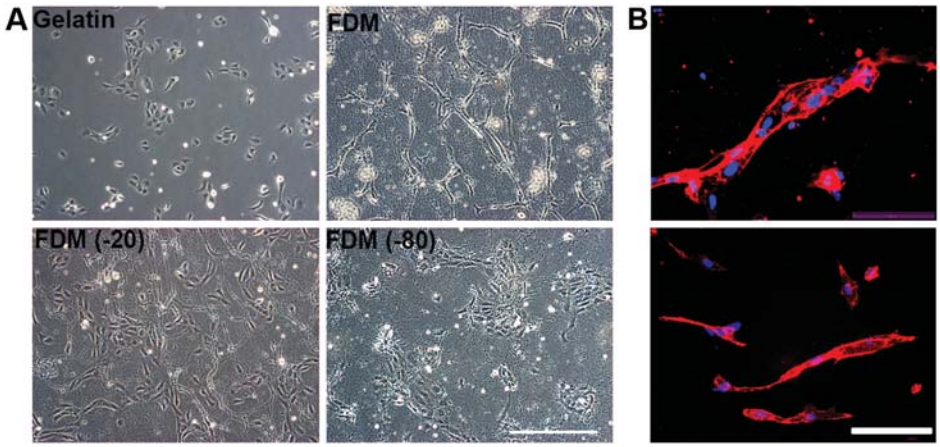

FIG. 6. CLS formation is independent of exogenous growth factors. Phase-contrast images of HUVECs cultured on each substrate for 24 h in EBM-2 medium without exogenous growth factors **(A)**. Scale bar is 200 μm. CLSs were detected on natural FDM when they were cultured with (*bottom*) or without (*top*) supplement. F-actin (*Red*), DAPI (*Blue*) (**B**). Scale bar is 100 μm. EBM-2, endothelial basal medium-2. Color images available online at www.liebertpub.com/tea

were cultured on. After cell culture for 24 h, cells were stained with Rhodamine phalloidin to visualize their cytoskeleton (Fig. 7A). Cells on soft substrate (natural FDM) showed branching, disorganized actin fiber, and high number of filopodia, whereas on the stiffer ones (gelatin and modified FDMs) exhibited less branching, organized actin fiber, and polygonal cell shape.[32] Based on the fluorescence images, we collected morphological information such as cell spreading area and circularity index. We found that MSCs spread almost equally on all substrates (Fig. 7B), but they formed different morphological features. Cells on physically modified FDMs and gelatin have higher circularity index than those found on natural FDM, but comparatively similar to those on gelatin (Fig. 7C). Our finding indicates that different substrate stiffness posed diverse cell shapes, which result in distinct actin organization. The correlation between cell shape and actin organization is strongly associated with cell growth, physiology, and fate determination.[8]

Meanwhile, the proliferation of MSCs was characterized at day 1 and 3 after culturing. On day 1, we observed that cell proliferation varied with a particular trend dependent on types of substrates. In the FDM groups, stiffer substrates with ECM composition and structures promote higher proliferation as opposed to softer ones.[17] This tendency was

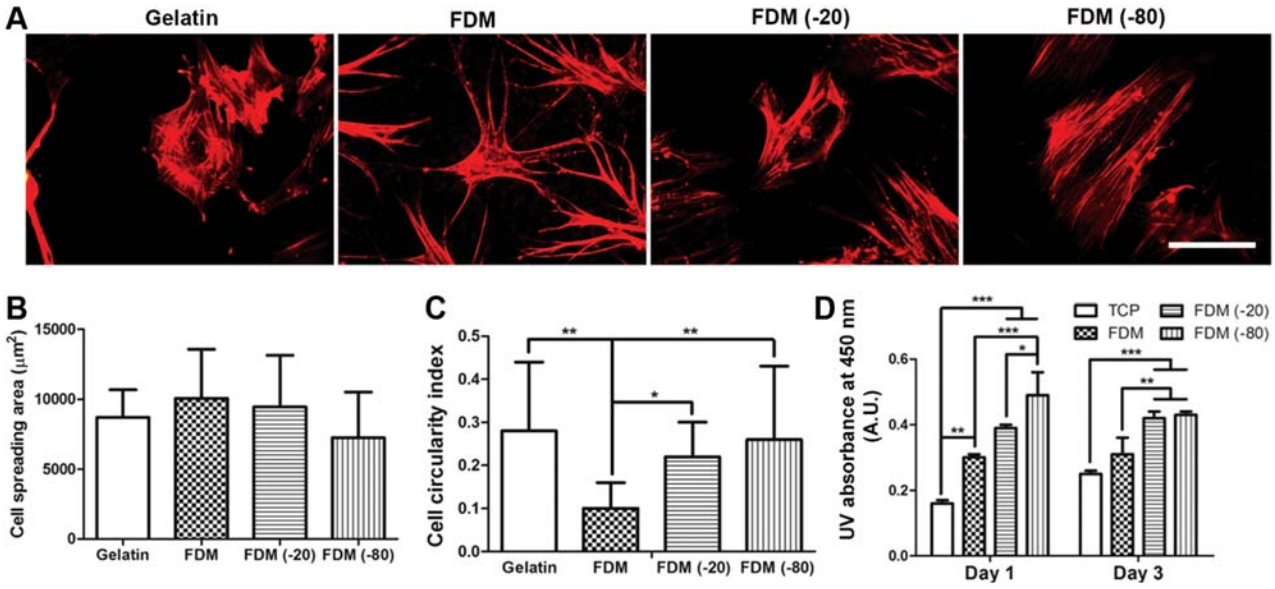

FIG. 7. Human MSC adhesion and morphology analysis. Human MSC morphology was visualized at 24 h by F-actin (*red*) and DAPI (*blue*) staining **(A)**. Scale bar is 100 μm. Cell morphology is quantitatively analyzed by two parameters: cell spreading area **(B)** and cell circularity **(C)**. Cell number at day 1 and day 3 is obtained by the CCK-8 assay **(D)**. Statistically significant difference among four groups is indicated as $*p<0.05$, $**p<0.01$, and $***p<0.001$. Color images available online at www.liebertpub.com/tea

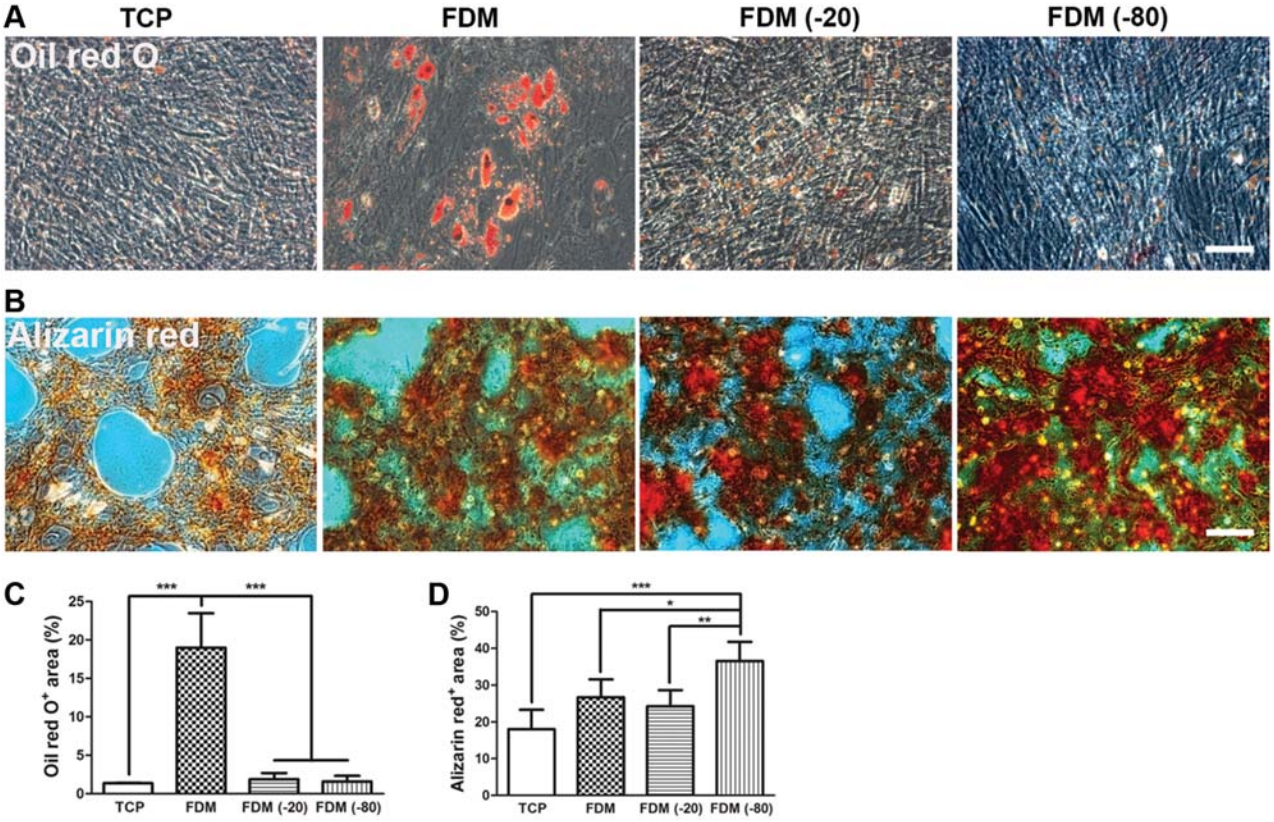

FIG. 8. Human MSC adipogenesis and osteogenesis. Human MSC adipogenic capacity on each substrate is evaluated by Oil red O staining **(A)**, while osteogenic is visualized by Alizarin red staining **(B)**. Oil red- **(C)** and Alizarin red- **(D)** stained positive percentage area is quantitatively analyzed using image J software. Scale bar is 100 μm. Statistically significant difference among four groups is indicated as $*p < 0.05$, $**p < 0.01$, and $***p < 0.001$. Color images available online at www.liebertpub.com/tea

maintained upon culture at day 3, showing substrate dependency for cell proliferation (Fig. 7D).

Following differentiations, cells were examined for deposition of lipid and calcium. Oil red O staining shows the formation of lipid droplets in all groups that indicates these cells have undergone adipogenesis (Fig. 8A). Accordingly, these cells were also responsive to osteogenic induction evidenced by mineralization of calcium as visualized by alizarin red (Fig. 8B). Quantitatively, MSCs on natural FDM with the lowest matrix elasticity have greater capability to differentiate into adipogenesis than the other stiffer substrates (Fig. 8C), whereas cells induced with the osteogenic medium showed that they were preferentially more competent on the stiffest FDM (−80) (Fig. 8D). For matrix elasticity perspectives, cells on TCP felt the stiffest environment, but the absence of ECM might be the main cause for the lower osteogenic induction on this group, relative to the physically modified FDMs. All of these results further confirmed the critical role of matrix elasticity in MSC multilineage specification.[32,33]

Physical modification on FDM induces the changes of both matrix structure and elasticity, and matrix elasticity changes are induced by matrix re-arrangement during physical treatment. Physically modified FDM showed different mechanical properties with YM ranging from less than 100 Pa to more than 4000 Pa. They can be used for various physiological applications as most organs and tissues are mechanically varied by nature ranging from 100 Pa for the brain to 100,000 Pa for soft cartilage.[34] Furthermore, the biophysical properties of substrates can influence cell morphology, proliferation, motility, and differentiation. Thus, physically modified FDMs can be used for studying the behavior and related mechanisms of HUVECs, hMSCs, and prospectively other type of cells. In addition, this study gives a very valuable instruction for the future application of natural ECMs that they are sensitive to storage temperature; ECMs should be maintained at a consistent condition according to different research purposes. On the other hand, in this study, our results suggest that matrix elasticity plays a critical role in regulating HUVEC and hMSC differentiation. However, after physical modification, the changes of calcium metabolism, pH, and other parameters in FDM may contribute to cell differentiation. Thus, a detailed examination on the effect of modified FDMs on cell differentiation deserves further exploration.

Conclusion

FDMs were physically modified by storing them at different temperatures. Interestingly, a facile freeze–thaw process induced significant changes of surface texture, topography, and matrix elasticity on FDM, as determined by FIB-CryoSEM and AFM. These changes subsequently caused notably different

responses of HUVECs and hMSCs cultured on them. HUVECs cultured on natural FDMs exhibited tip cell-like characters; they carried more filopodia and expressed a higher level of *MT1-MMP* with higher motility. This was sharply contrasted with HUVECs cultured on physically modified FDMs that they showed a stalk cell-like property proliferating faster and establishing tight junction with neighbor cells. This study shows that physical modification impairs the usual vascular morphogenesis on FDMs and this result is correlated with increase of matrix elasticity after physical modification. The improved adipogenesis level of hMSCs on natural FDMs with lower matrix elasticity and acceleration of osteogenesis on physically modified FDM further confirmed the important role of matrix elasticity on stem cell lineage specification. However, additional work is needed to understand the mechanism of freeze–thaw-induced biomechanical property changes on FDMs and the related molecular pathway that regulates cellular behavior changes on FDMs.

Acknowledgments

This work was supported by research resettlement fund for the new faculty of Seoul National University, and by a grant of the Korean Health Technology R&D Project (A120216), Ministry of Health and Welfare, Republic of Korea.

Disclosure Statement

No competing financial interests exist.

References

1. Soucy, P.A., and Romer, L.H. Endothelial cell adhesion, signaling, and morphogenesis in fibroblast-derived matrix. Matrix Biol **28,** 273, 2009.
2. Hielscher, A.C., Qiu, C., and Gerecht, S. Breast cancer cell-derived matrix supports vascular morphogenesis. Am J Physiol Cell Physiol **302,** C1243, 2012.
3. Du, P., Subbiah, R., Park, J.H., and Park, K. Vascular morphogenesis of human umbilical vein endothelial cells on cell-derived macromolecular matrix microenvironment. Tissue Eng Part A **20,** 2365, 2014.
4. Bae, S.E., Bhang, S.H., Kim, B.S., and Park, K. Self-assembled extracellular macromolecular matrices and their different osteogenic potential with preosteoblasts and rat bone marrow mesenchymal stromal cells. Biomacromolecules **13,** 2811, 2012.
5. Haag, J., Baiguera, S., Jungebluth, P., Barale, D., Del Gaudio, C., Castiglione, F., Bianco, A., Comin, C.E., Ribatti, D., and Macchiarini, P. Biomechanical and angiogenic properties of tissue-engineered rat trachea using genipin cross-linked decellularized tissue. Biomaterials **33,** 780, 2012.
6. Miron-Mendoza, M., Seemann, J., and Grinnell, F. The differential regulation of cell motile activity through matrix stiffness and porosity in three dimensional collagen matrices. Biomaterials **31,** 6425, 2010.
7. Sun, H.L., Zhu, F., Hu, Q., and Krebsbach, P.H. Controlling stem cell-mediated bone regeneration through tailored mechanical properties of collagen scaffolds. Biomaterials **35,** 1176, 2014.
8. Mammoto, A., Connor, K.M., Mammoto, T., Yung, C.W., Huh, D., Aderman, C.M., Mostoslavsky, G., Smith, L.E., and Ingber, D.E. A mechanosensitive transcriptional mechanism that controls angiogenesis. Nature **457,** 1103, 2009.
9. Ma, Z.W., Mao, Z.W., and Gao, C.Y. Surface modification and property analysis of biomedical polymers used for tissue engineering. Colloids Surf B Biointerfaces **60,** 137, 2007.
10. Kumar, A., and Srivastava, A. Cell separation using cryogel-based affinity chromatography. Nat Protoc **5,** 1737, 2010.
11. Venkatasubramanian, R.T., Wolkers, W.F., Shenoi, M.M., Barocas, V.H., Lafontaine, D., Soule, C.L., Iaizzo, P.A., and Bischof, J.C. Freeze-thaw induced biomechanical changes in arteries: role of collagen matrix and smooth muscle cells. Ann Biomed Eng **38,** 694, 2010.
12. Zhao, X., Kim, J., Cezar, C.A., Huebsch, N., Lee, K., Bouhadir, K., and Mooney, D.J. Active scaffolds for on-demand drug and cell delivery. Proc Natl Acad Sci U S A **108,** 67, 2011.
13. Wen, J.H., Vincent, L.G., Fuhrmann, A., Choi, Y.S., Hribar, K.C., Taylor-Weiner, H., Chen, S.C., and Engler, A.J. Interplay of matrix stiffness and protein tethering in stem cell differentiation. Nat Mater **13,** 979, 2014.
14. Stroka, K.M., and Aranda-Espinoza, H. Effects of morphology vs. cell-cell interactions on endothelial cell stiffness. Cell Mol Bioeng **4,** 9, 2011.
15. Saunders, R.L., and Hammer, D.A. Assembly of human umbilical vein endothelial cells on compliant hydrogels. Cell Mol Bioeng **3,** 60, 2010.
16. Krishnan, R., Klumpers, D.D., Park, C.Y., Rajendran, K., Trepat, X., van Bezu, J., van Hinsbergh, V.W.M., Carman, C.V., Brain, J.D., Fredberg, J.J., Butler, J.P., and Ameron gen, G.P.V. Substrate stiffening promotes endothelial monolayer disruption through enhanced physical forces. Am J Physiol Cell Physiol **300,** C146, 2011.
17. Deroanne, C.F., Lapiere, C.M., and Nusgens, B.V. In vitro tubulogenesis of endothelial cells by relaxation of the coupling extracellular matrix-cytoskeleton. Cardiovasc Res **49,** 647, 2001.
18. Liliensiek, S.J., Wood, J.A., Yong, J., Auerbach, R., Nealey, P.F., and Murphy, C.J. Modulation of human vascular endothelial cell behaviors by nanotopographic cues. Biomaterials **31,** 5418, 2010.
19. Jeon, H., Tsui, J.H., Jang, S.I., Lee, J.H., Park, S., Mun, K., Boo, Y.C., and Kim, D.H. Combined effects of substrate topography and stiffness on endothelial cytokine and chemokine secretion. ACS Appl Mater Interfaces **7,** 4525, 2015.
20. Wood, J.A., Liliensiek, S.J., Russell, P., Nealey, P.F., and Murphy, C.J. Biophysical cueing and vascular endothelial cell behavior. Materials **3,** 1620, 2010.
21. Gasiorowski, J.Z., Liliensiek, S.J., Russell, P., Stephan, D.A., Nealey, P.F., and Murphy, C.J. Alterations in gene expression of human vascular endothelial cells associated with nanotopographic cues. Biomaterials **31,** 8882, 2010.
22. Dreier, B., Gasiorowski, J.Z., Morgan, J.T., Nealey, P.F., Russell, P., and Murphy, C.J. Early responses of vascular endothelial cells to topographic cues. Am J Physiol Cell Physiol **305,** C290, 2013.
23. Potente, M., Gerhardt, H., and Carmeliet, P. Basic and therapeutic aspects of angiogenesis. Cell **146,** 873, 2011.
24. Li, S., Huang, N.F., and Hsu, S. Mechanotransduction in endothelial cell migration. J Cell Biochem **96,** 1110, 2005.
25. Lamalice, L., Le Boeuf, F., and Huot, J. Endothelial cell migration during angiogenesis. Circ Res **100,** 782, 2007.
26. Jin, F.Y., Hagemann, N., Schafer, S.T., Brockmeier, U., Zechariah, A., and Hermann, D.M. SDF-1 restores angiogenesis synergistically with VEGF upon LDL exposure

despite CXCR4 internalization and degradation. Cardiovasc Res **100,** 481, 2013.
27. Sun, J., Li, Y.H., Graziani, G.M., Filion, L., and Allan, D.S. E-selectin mediated adhesion and migration of endothelial colony forming cells is enhanced by SDF-1 alpha/CXCR4. PLoS One **8,** e60890, 2013.
28. van Hinsbergh, V.W.M., Engelse, M.A., and Quax, P.H.A. Pericellular proteases in angiogenesis and vasculogenesis. Arterioscl Throm Vas **26,** 716, 2006.
29. Davis, G.E. Angiogenesis and proteinases: influence on vascular morphogenesis, stabilization and regression. Drug Discov Today Dis Models **8,** 13, 2011.
30. Solon, J., Levental, I., Sengupta, K., Georges, P.C., and Janmey, P.A. Fibroblast adaptation and stiffness matching to soft elastic substrates. Biophys J **93,** 4453, 2007.
31. Discher, D.E., Janmey, P., and Wang, Y.L. Tissue cells feel and respond to the stiffness of their substrate. Science **310,** 1139, 2005.
32. Engler, A.J., Sen, S., Sweeney, H.L., and Discher, D.E. Matrix elasticity directs stem cell lineage specification. Cell **126,** 677, 2006.
33. Chen, G., Dong, C., Yang, L., and Lv, Y. 3D scaffolds with different stiffness but the same microstructure for bone tissue engineering. ACS Appl Mater Interfaces **7,** 15790, 2015.
34. Levental, I., Georges, P.C., and Janmey, P.A. Soft biological materials and their impact on cell function. Soft Matter **3,** 299, 2007.

Address correspondence to:
Kangwon Lee, PhD
Program in Nanoscience and Technology
Graduate School of Convergence Science and Technology
Seoul National University
Seoul 08826
Republic of Korea

E-mail: kangwonlee@snu.ac.kr

Kwideok Park, PhD
Center for Biomaterials
Korea Institute of Science and Technology
Seoul 02792
Republic of Korea

E-mail: kpark@kist.re.kr

Received: November 3, 2015
Accepted: January 11, 2016
Online Publication Date: February 24, 2016